Mechanical Strength of Nano-Elements

Takayuki Kitamura[1, a], Hiroyuki Hirakata[2,b], Takashi Sumigawa[1,c], and Takahiro Shimada[1,d]

[1] Department of Mechanical Engineering and Science, Kyoto University, Kyoto 606-8501, Japan

[2] Department of Mechanical Engineering, Osaka University, Suita, Osaka, 565-0871, Japan

[a]kitamura@kues.kyoto-u.ac.jp, [b]hirakata@mech.eng.osaka-u.ac.jp

[c]sumigawa@cyber.kues.kyoto-u.ac.jp, [d]shimada@cyber.kues.kyoto-u.ac.jp

Keywords: Nano-elements, Deformation, Fracture, Mechanical properties, Multi-physics properties

Abstract The focus in this project is put on the mechanical property of nano-elements. The deformation property of a thin film consisting discretely arrayed nano-elements on a substrate is evaluated by means of an atomic force microscope (AFM) with a loading apparatus, and a novel experimental technique for a single nano-element is proposed. Moreover, the fact that the thin film eliminates stress singularity at the interface edge between dissimilar materials is numerically and experimentally elucidated. We also investigate the microscopic switching mechanism in ferroelectric domains from the atomistic point of view using first-principles calculations.

Introduction

New deposition techniques enable us to fabricate nano-sized structures. In particular, a thin film consisting of nano-elements is formed on a substrate by means of the dynamic oblique deposition (DOD) [1-2]. It has the potential to play a key role in mechanical electronic devices because the thin films would exhibit significantly characteristic mechanical properties in comparison with solid films. The geometrical anisotropy of constituent nano-elements would cause the mechanical anisotropy of film, and insertion of the thin film between dissimilar materials as an interface layer may break down a continuum approximation of the stress field near the interface owing to discrete structure of the film. However, the investigation of the mechanical properties of nano-elements has not been enough yet.

In this paper, we review our experimental and theoretical works on the mechanical properties of nano-elements. In addition, the coupling effects of mechanical deformation and ferroelectricity, namely, multi-physics properties in nano-structured ferroelectrics are investigated, as well.

Mechanical property of thin film consisting of nanosprings [3-4]

Experimental procedure. As a base layer, a Ta_2O_5 solid film is deposited on a silicon (100) substrate by electron beam (EB) evaporation. Then, nanosprings (helical nano-elements) of Ta_2O_5 are grown by the dynamic oblique deposition (DOD). A Ta_2O_5 cap layer with a thickness of 280 nm is deposited on the nanosprings. Figure 1(a) shows a scanning electron micrograph of the multi-layered thin films. The height of the nanosprings, h_s, is 560 nm. The areal number density of springs is 65 per μm^2. The number of turns, the outside radius, and diameter of wire of the nanospring are 3.5, 75 nm, and 60±10 nm, respectively.

Figure 1(b) shows the specimen configuration. Specimens for the loading tests are cut from the multi-layered thin films by a focused ion beam (FIB). Several specimens with different areas (S = 1.9-13.2 μm^2) are prepared.

The tests are conducted using an atomic force microscope with a loading apparatus (Hysitron: Triboscope). Figures 1(c) and 1(d) schematize the loading test. The vertical and lateral forces, F_v and

F_l, are applied to the cap layer by the diamond tip. In the vertical loading tests, the vertical force is applied to the cap layer at a constant loading velocity of 10 μN/s (see Fig. 1(c)). In the lateral loading tests, the lateral force is applied to the side edge of the cap layer (see Fig. 1(d)). The loading tip is moved along the substrate surface toward the specimen at a constant velocity of 5 nm/s.

Results. Figure 2(a) plots the F_v against the vertical displacement, δ_v, for a specimen with $S = 3.3$ μm^2. The fact that the relation between F_v and δ_v is almost linear indicates that the specimen deforms elastically. The vertical stiffness of the thin film, K_v ($=F_v/\delta_v$), is evaluated by the least-squares approximation. The relationship between K_v and S is shown by solid circles in Fig. 2(c). K_v has an almost linear relationship with S. The apparent Young's modulus, E', and stiffness constant, k_v, of a spring are defined as $E' = K_v (h_s/S)$ and $k_v = K_v/m$, respectively. The mean values of E' and k_v obtained from the vertical loading tests are 0.375 GPa and 10.29 N/m, respectively.

Figure 2(b) shows the F_l plotted against the lateral displacement, δ_l, in the lateral loading test of a specimen with $S = 6.4$ μm^2. F_l increases almost linearly with δ_l. The lateral stiffness of the thin film, K_l ($=F_l/\delta_l$), is evaluated. The open squares in Fig. 2(c) show the relationship between K_l and S. K_l increases almost linearly with increasing S. The apparent shear modulus of the thin film, G', and the lateral stiffness measurement, k_l, of a spring are defined as $G' = K_l (h_s/S)$ and $k_l = K_l/m$, respectively. The mean values of G' and k_l obtained from the lateral loading tests are 0.060 GPa and 1.66 N/m, respectively.

The E' and G' of the thin film consisting of Ta_2O_5 nanosprings are 2-3 orders of magnitude lower than those of the solid Ta_2O_5 film ($E \approx 117$ GPa and $G \approx 47$ GPa). The ratio of E' to G' is 6.2, while that of isotropic solid materials given as $2(1+\nu)$ must be at most 3.0 because the maximum value of ν is 0.5. This means that the thin film composed of Ta_2O_5 helical nanosprings has a strong anisotropy.

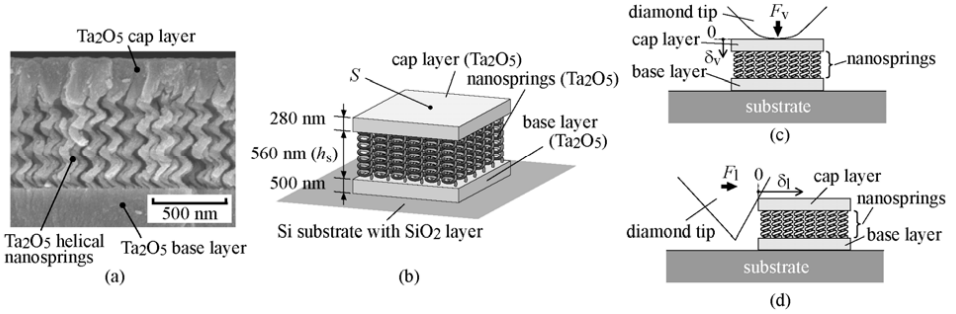

Fig.1 (a) SEM micrograph of multi-layered thin films. (b) Configuration of specimen. (c) Vertical loading method. (d) Lateral loading method.

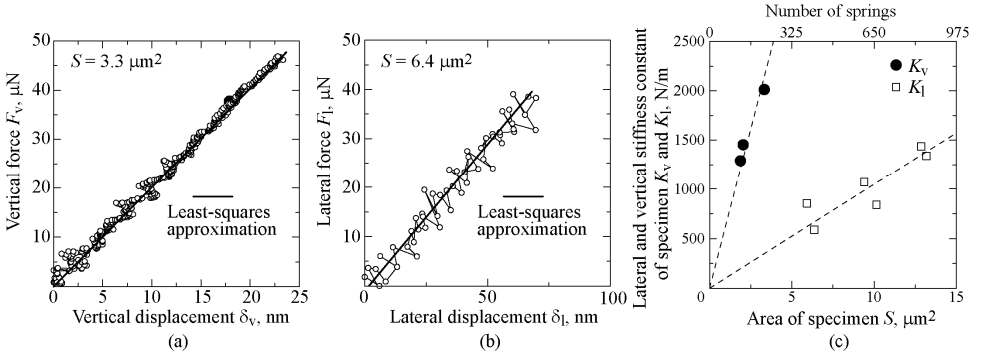

Fig.2 Relationship between force and displacement: (a) Vertical loading method, (b) Lateral loading method. (c) Relationship between stiffness and area of specimen.

Proportion of experimental technique for single nanocolumn[5]

Experimental procedure. Nanocolumns (cylindrical nano-elements) are grown by the high temperature glancing angle deposition (HT-GLAD). Al (purity: 99.999%) is deposited on the flat top of a gold wire by EB evaporation. During the deposition, the temperature of the wire is kept constant at 673±10 K. Figure 3(a) shows the nanocolumn used for compression test, which has a diameter of about 60 nm. Figure 3(b) shows the configuration of the gold wire and a diamond loading tip attached to a micro load sensor. The wire can be driven by a piezoelectric actuator. The piezo displacement in the y-direction, u_y, is monotonically increased at a rate of 4 nm/s toward the target whisker, and a compressive load, P, is then applied to the whisker by a flat face of the loading tip. The *in-situ* observation is conducted by a TEM (JEOL Ltd., JEM-2100) with an electron beam energy of 200 kV under a vacuum (1.5×10^{-5} Pa).

Results. Figure 3(c) shows the P-u_y curve where the nominal stress and strain are indicated on the right and the top axes, respectively. The stress and the strain are evaluated in terms of the original area and the length of the nanocolumn. The curve is characterized by a sharp yield point (B), an extensive easy glide region (C-G), and a strong work-hardening region (G-I). Immediately after the start of load application, the stress increases linearly with strain, and reaches the yielding point. The macroscopic yield stress is estimated at about 750 MPa. After the sudden drop after point B, the stress generally continues to be flat with remarkable serrations between 200 MPa and 750 MPa. The increment of strain in the region is about 0.25. After this region, the stress increases rapidly with strong work-hardening.

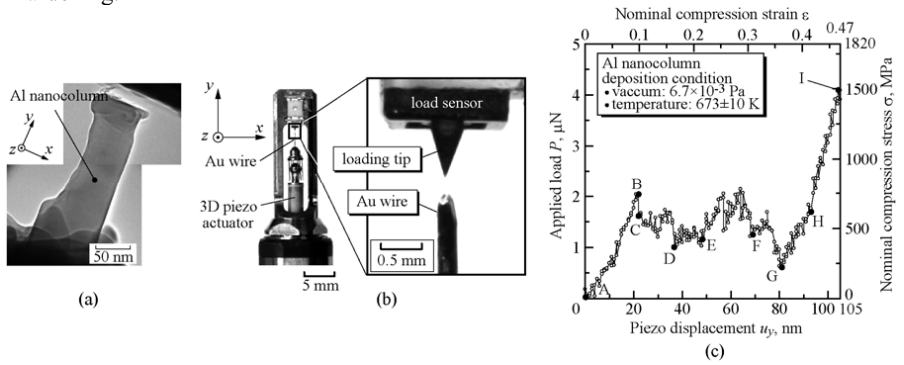

Fig.3 (a) TEM micrograph of Al nanocolumn. (b) Configuration of wire and loading tip. (c) Relationship between applied load, P, and piezo displacement in y-direction, u_y.

Effect of thin film consisting of nanosprings on stress fields at interface edge and crack tip [4]

Analytical procedure. Stress analysis is conducted under plane strain condition through FEM using ABAQUS 6.5. Each nanospring is replaced by the equivalent cylindrical beam with a height of h_b=560 nm, a diameter of D_b = 259 nm, and a Young's modulus of E_b 0.11 GPa. The D_b and E_b can be derived from the vertical and lateral stiffness measurements of a single spring, k_v and k_l.

Figure 4 shows the model used for analyzing the stress distribution near the interface edges between the thin film and a solid body. The thin film consisting of Ta_2O_5 nanosprings with a thickness of 560 nm is sandwiched between an elastic solid body and a substrate. Figure 4(c) shows the mesh division for the models. Two types of models with different interface edges between the thin film and the solid body are prepared. One has a free edge where the surface-interface angle is 90°–90° (see Fig. 5(a)), and the other has an interface crack with a length of 4 μm (see Fig. 4(b)). The Young's modulus and Poisson's ratio of the Ta_2O_5 solid body are 117 GPa and 0.23, respectively. The distance between springs is 125 nm, which is derived from the areal number density of springs. In addition,

models without nanosprings are prepared for comparison (Figs. 4(d), (e), and (f)). The models with and without the thin film consisting of nanosprings are designed as "spring model" and "non-spring model", respectively. The uniform displacement Δu_z is applied to the top of the model.

Results. The stresses in the elements of the elastic solid body along the interface are extracted. Figures 5(a) and (b) show the distributions of the normal stresses, σ_x and σ_z, and the shear stress, τ_{zx}, along the interface in the models with a free edge. The stresses are normalized by the z-directional normal stress at the center of the interface, σ_0, in each model. In the no-spring model (Fig. 5(a)), the stresses increase near the free edge. A stress singularity represented by $\sigma_{ij}/\sigma_0 = K/r^{\lambda}$ $(i, j = z, x)$ [6] is observed near the free edge in each distribution curve. Here, K is the stress intensity factor, r is the distance from the free edge, and λ is a parameter that depends on the materials and the edge geometry. In the spring model (Fig. 5(b)), there is no stress singularity near the free edge.

Figures 5(c) and (d) show the distributions of the normalized stresses along the interface in the models containing an interface crack. In the non-spring model (Fig. 5(c)), the stresses are concentrated in the region near the crack tip. Stress singularity is observed near the crack tip. In the spring model (Fig. 5(d)), σ_z and τ_{zx} are almost constant over the interface as in the case of the model with the free edge. No singular stress field occurs in any of the distributions.

The stress concentration at the free edge of an interface is induced by the mismatch of deformation on the interface. The mismatch is mainly due to the difference in Poisson's contractions between the different components. Since nanosprings are oriented vertically on the substrate and are separated from each other, the in-plane deformation of the thin film follows that of the adjoining component on the interface. In short, the difference of Poisson's contractions for the vertical deformation is zero. The stress concentration at the interface crack tip is induced by not only the mismatch of deformation on the interface but also the traction force from above and below the crack. However, no traction force is exerted on the crack tip in the spring model because the under part of the crack is constitutively separated from the crack tip.

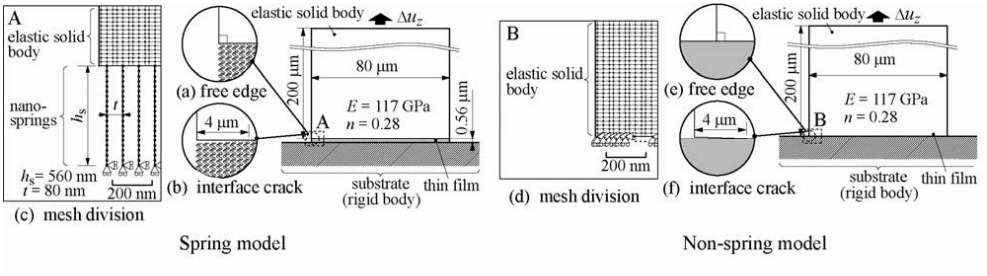

Fig. 4 Analytical models for FEM.

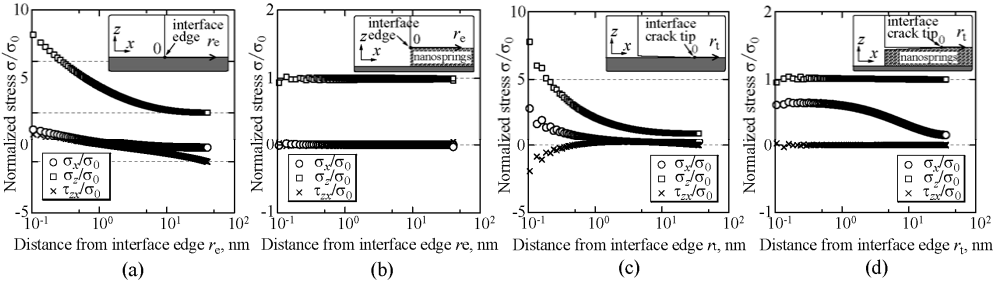

Fig. 5 Distribution of normal stresses, σ_z and σ_x, and shear stress, τ_{zx}, along the interface: (a) near the interface edge in non-spring model, (b) near the interface edge in spring model, (c) near the interface crack tip in non-spring model, (b) near the interface crack tip in spring model.

Effect of thin film consisting of nanosprings on crack initiation at interface edge [7]

Experimental procedure A thin film consisting of Ta_2O_5 nanosprings is formed on a Si substrate by means of the DOD. A Ta_2O_5 solid film with a height of 1700 nm is then deposited on the thin film by the EB evaporation (see Fig. 6(a)). The number of turns, the outside radius, and diameter of wire of the nanospring are 3.5, 90 nm, and 40±10 nm, respectively.

The material is cut to a square coupon with a size of 5 mm×5 mm. A stainless cantilever is bonded to the thin film of the coupon using an epoxy adhesive. The thin film except the bonded region is mechanically removed.

Figures 6(b) and (c) illustrates the specimen configuration and the loading method. We carry out two types of experiments, which are designated as "Type A test" and "Type B test", respectively. Table 1 lists the sizes of the specimens. A vertical load applied to the lower face of the stainless steel cantilever (Fig.6 (b)) initiates a crack at the left edge of the thin film. On the other hand, a vertical load applied to the upper face of the cantilever (Fig.6(b)) initiates a crack at the right edge of the thin film.

The experiments are conducted at a room temperature in an air by means of a loading machine with an electromagnetic actuator. The vertical load is applied to the stainless cantilever at the point of l from the edge of the thin film with a constant displacement rate of 50 μm/s.

Analytical procedure Figure 7 illustrates mesh divisions for analytical models. The nanosprings are translated to equivalent beam elements. The Young's modulus and Poisson's ratio of the Ta_2O_5 solid body are 117 GPa and 0.23, respectively. In addition, models where the Ta_2O_5 solid film is directly laminated on the Si substrate without the thin film are analyzed for comparison. Hereafter, the analytical models with and without the thin film are designated as "thin film model" and "non-thin film model", respectively.

Results In the experiments, the displacement at the loading point, u_y, increases linearly with increasing the applied load, P. The sharpen drop of the load at the maximum value points out that the interface crack is initiated.

Figure 8(a) shows the typical relationship between the normal stress, σ_y, and the distance from the interface edge, x, at the crack initiation in the non-thin film model. σ_y is extracted from the elements adjoining the interface in the Si substrate. No stress singularity takes place at the left edge of the interface with the 90°-90°interface edge shape of the Ta_2O_5 solid film and the Si substrate (Type A). On the other hand, the right edge of the interface where the interface edge shape is 90°-180° generates a stress singularity due to the edge shape (Type B).

Figure 8(b) shows the typical relationship between the apparent normal stress of the nanospring, σ', and the distance from the interface edge, x, at the crack initiation in the thin film model. Using the longitudinal displacement of the nanospring, λ, the height, h_s, the Young's modulus, E_b, the diameter, D_b of the beam element, and the outer diameter of the nanospring, d, the apparent normal stress, σ', in the longitudinal direction of the nanospring is represented as follow:

$$\sigma' = (E_b\lambda/h_s)(D_b^2/d^2). \quad (1)$$

In Fig. 8(b), the stresses near the edge are nearly constant. The no strong stress concentration points out that the thin film consisting of nanosprings eliminates the stress singularity. Moreover, the stress distribution curves of all specimens show a good agreement near the interface edge. This signifies that the stress near the edge dominates the crack initiation. The magnitude of critical stress is evaluated as 78.5±4.0 MPa (ε_C'=5.1±0.2 ×10^{-2}).

Table 1 Dimensions of specimens used for the crack initiation experiment. Dimensions are in mm.

	L	*b*	*t*	*l*
A-1	2.27	1.58	1.92	17.5
A-2	2.17	2.09	1.87	11.0
A-3	1.37	1.77	1.90	15.5
B-1	1.74	1.68	1.90	15.5
B-2	1.85	1.95	1.89	16.0

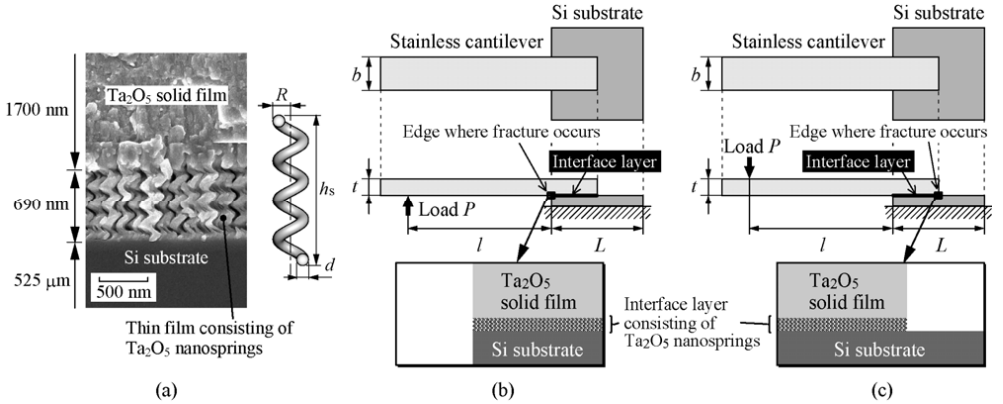

Fig. 6 (a) SEM micrograph of dissimilar material including a thin film comprising of Ta_2O_5 nanosprings. (b), (c) Illustrations of specimen and loading method.

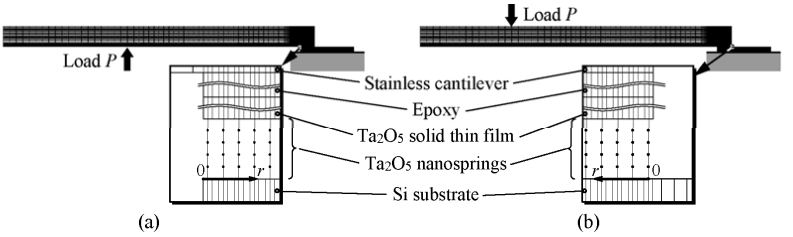

Fig. 7 Mesh division for FEM analysis: Type A test, and (b) Type B test.

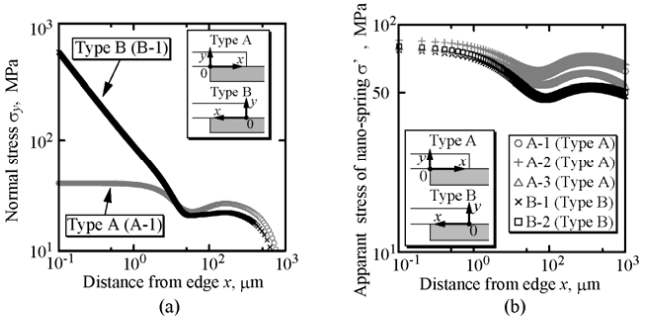

Fig. 8 Relationship between normal stress, σ, and distance from the edge of thin film, *r*: (a) non-thin film model, and (b) thin film model.

Multi-physics analysis based on first-principles calculations: Domain switching in $PbTiO_3$

Simulation procedure. First-principles calculations within the local density approximation are conducted using VASP, which employs the PAW (Projector Augmented Wave) pseudopotentials. Figure 9 shows the simulation model of 90° domain wall (DW) in $PbTiO_3$. The equilibrium structure is obtained by fully relaxing atoms using the conjugate gradient method. We, then, apply a small shear strain, $\Delta\gamma_{xz}$, to the simulation cell step by step. At each strain, internal atoms are fully relaxed by the same manner as described above.

Results. Figure 10(a) plots stress-strain curve under shear. After the stress reaches the maximum of 152 MPa, it drops dramatically, suggesting that the system becomes unstable. Figure 10(b) shows change in site-by-site polarization distribution near the DW under shear. The Pb-Ti-O plane number corresponds to that in Fig. 9. The shear deformation is localized in the vicinity of the DW, between the "-1" and "2" planes. At the point where stress drops, polarization direction on "-1" plane rotates from right-up to right-down. As a result, the DW propagates in the direction normal to the wall, indicating stress-induced domain switching. Hence, the maximum stress of 152 MPa is the critical shear stress for domain switching. Figure 11 depicts change in atomistic and electronic structures during domain switching. The Pb-O covalent bond emphasized by white lines is switched from α to β site, accompanying movement of the DW. Thus, we demonstrate that the bond reconstruction is responsible for domain switching. For more details and other applications, please see Refs. [8-10].

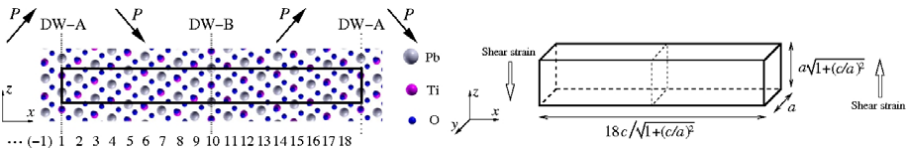

Fig. 9 Simulation model of 90° domain wall in $PbTiO_3$ (a=0.3867 nm and c=0.4034 nm).

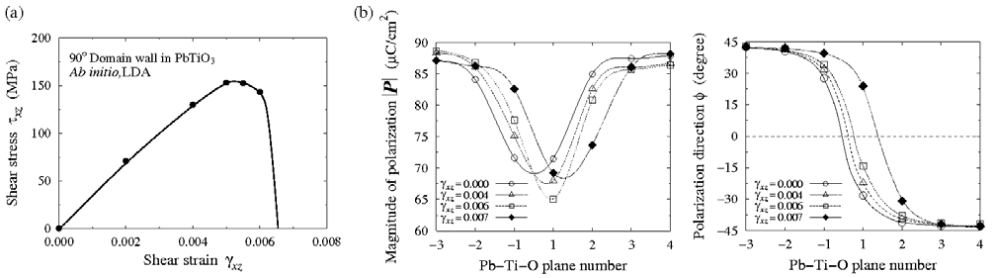

Fig. 10 (a) Stress-strain curve. (b) Change in local polarization distribution across a DW under shear.

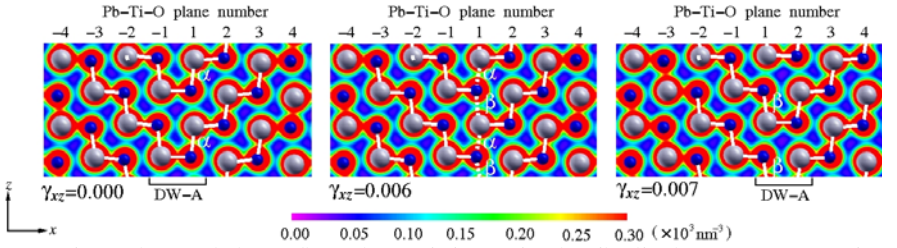

Fig. 11 Change in atomistic configuration and charge density distribution near a DW under shear.

Summary

The mechanical properties of nano-elements have been investigated in this project. Novel experiments and stress analyses for the nano-elements elucidate the specific behavior of deformation and fracture. Furthermore, first-principles calculations reveal the fundamental mechanism of domain switching from the atomistic point of view. The main results obtained are summarized as follows.

(1) Apparent Young's modulus, E', and shear modulus of a thin film consisting of Ta_2O_5 nanosprings are evaluated as 0.375 and 0.060, respectively. These values are 2-3 orders of magnitude smaller than those of a conventional Ta_2O_5 solid thin film. Moreover, the thin film has a strong deformation anisotropy which solid materials cannot attain.

(2) Vertical stiffness k_v and lateral stiffness, k_l, of the single Ta_2O_5 nanospring are evaluated as 10.29 and 1.66 N/m, respectively.

(3) We proposed an experimental technique for evaluating the deformation behavior of a single nanocolumn.

(4) No stress singularity is found near the free edge of an interface and near the interface crack tip between the thin film consisting of nanosprings and an elastic solid body. The marked stress relaxation is due to the discrete structure of the thin film.

(5) Elimination of the stress singularity owing to the thin film consisting of nanosprings is experimentally demonstrated. The crack initiation at the interface edge is dominated by the apparent stress of the nanospring.

(6) We reveal the stress-induced switching mechanism of 90° domain wall in $PbTiO_3$ using first-principles calculations. The critical shear stress is evaluated to be 152 MPa.

References

[1] M. Suzuki and Y. Taga: Japanese Journal of Applied Physics Vol. 40 (2001), p. L358.

[2] K. Robbie, M.J. Brett and A. Lakhtakia: J Vacuum Sci Technol Vol. A13(6) (1995), p. 2991.

[3] H. Hirakata, S. Matsumoto, M. Takemura, M. Suzuki and T. Kitamura: International Journal of Solids and Structures Vol. 44 (2007), p. 4030.

[4] T. Sumigawa, H. Hirakata, M. Takemura, S. Matsumoto, M. Suzuki and T. Kitamura: Engineering Fracture Mechanics Vol. 75 (2008), p. 3073.

[5] Y. Takahashia, T. Sumigawa, H. Hirakata, M. Takemura, M. Suzuki and T. Kitamura: Materials Science & Engineering A, submitted.

[6] D.B. Bogy, Journal of Applied Mechanics Vol. 35 (1968), p. 460.

[7] T. Sumigawa, T. Sueta, Y. Futamura, M. Suzuki and Takayuki Kitamura: Engineering Fracture Mechanics, submitted.

[8] T. Shimada, Y. Umeno and T. Kitamura: Phys. Rev. B Vol. 77 (2008), art. 094105.

[9] Y. Umeno, T. Shimada, T. Kitamura and C. Elsässer: Phys. Rev. B Vol. 74 (2006), art. 174111.

[10] T. Kitamura, Y. Umeno, F. Shang, T. Shimada and K. Wakahara: J. Solid Mech. Mater. Eng. Vol. 1 (2007), p. 1423.